J Therm Spray Tech (2020) 29:241–254
https://doi.org/10.1007/s11666-019-00947-0

PEER REVIEWED

# Icephobic Behaviour and Thermal Stability of Flame-Sprayed Polyethylene Coating: The Effect of Process Parameters

**Valentina Donadei[1] · Heli Koivuluoto[1] · Essi Sarlin[1] · Petri Vuoristo[1]**

Submitted: 28 June 2019 / in revised form: 21 October 2019 / Published online: 11 November 2019


**Abstract** The present work investigates the effect of different process parameters on the production of low-density polyethylene (LDPE) coatings by flame spray technology. Previously, flame spraying of polymers has been successfully performed to obtain durable icephobic coatings, providing an interesting solution for applications facing icing problems, e.g. in marine, aviation, energy, and transportation industry. However, the fine tailoring of the process parameters represents a necessary strategy for optimising the coating production due to the unique thermal properties of each polymer. For this purpose, we vary the heat input of the process during flame spraying of the coating, by changing the transverse speed and the spraying distance. The results show that the variation in the process parameters strongly influenced the quality of the polymer coating, including its areal roughness, thickness, chemical composition, thermal stability, and degree of crystallinity. Furthermore, we demonstrate that these properties significantly affect the icephobic behaviour of the surface within the spray window of the chosen parameters. In conclusion, the relationship between the thermal degradation of the polymer and the icephobicity of the surface was defined. This highlights the importance of process parameter optimisation in order to achieve the desired icephobic performance of the LPDE coatings.

**Keywords** flame spraying · ice adhesion strength · icephobic surface · polymer coating · thermal degradation

## Introduction

The accumulation of ice and snow on outdoor structures represents a serious problem in Nordic regions as well as in several countries in both hemispheres (Ref 1). In fact, the atmospheric ice strongly adheres to bare surfaces and its accumulation contributes to compromising the effectiveness and efficiency of different applications, for example, power lines and electrical conductors during winter storms (Ref 2). Moreover, ice accretion on aircraft surfaces produces severe changes in their aerodynamic properties (Ref 3). Since the accumulation of ice represents an adverse impact on both safety and structure performances (Ref 4, 5), different strategies are developed to prevent ice adhesion on outdoor surfaces. Several active and passive methods have been adopted to avoid ice accumulation and reduce safety issues. On one hand, active methods include processes involving the mechanical removal of ice by scraping and vibrating the structure, the use of de-icing chemical fluids, and thermal heating above the freezing point (Ref 6). Unfortunately, these active methods produce environmental pollution, energy consumption, and ineffective manual operations. On the other hand, passive methods represent a smart strategy, which aims to develop efficient and durable anti-ice solutions. These methods consist of using icephobic material to coat the ice-exposed surfaces, preventing ice accumulation and consequent safety issues. Theoretically, the surface is considered as icephobic when it effectively reduces the adhesion strength of ice and prevents ice accumulation (Ref 7). In particular, the adhesion forces should be low in order to practically

This article is an invited paper selected from presentations at the 2019 International Thermal Spray Conference, held May 26-29, 2019 in Yokohama, Japan and has been expanded from the original presentation.

✉ Valentina Donadei
valentina.donadei@tuni.fi

[1] Faculty of Engineering and Natural Sciences, Tampere University, P.O. Box 589, FI-33014 Tampere, Finland

shed the ice off from the surface (Ref 8). However, only a few coatings have been achieved this, withstanding their durability (Ref 9).

The research and development of icephobic surfaces have been achieved a considerable interest in the speciality of coating design, during the last two decades (Ref 10, 11). Different coating technologies have been used for the production of icephobic surfaces, mainly chemical synthesis (Ref 12), sol–gel methods (Ref 13), and other laboratory-scale coating and painting processes. However, these methods generally require extended processing time, a large waste of chemicals, and controlled environmental conditions. Therefore, thermal spray technology represents a valid alternative to the chemical synthesis for the production of smart coatings (Ref 14). This technique aims to improve the performance of a component by adding a functionalised coating to the surface (Ref 15). Anti-corrosion (Ref 16-19), low friction and wear resistance (Ref 20-23), chemical and weathering resistance (Ref 24, 25), and antifouling (Ref 26, 27) represent some of the applications of the thermally sprayed coatings. In particular, flame spraying represents one of the thermal spray techniques used for the production of polymer coatings. In this process, the material in the form of powder is fed into a spray gun. The powder is injected into a combustion flame, which is used to melt the thermoplastic polymers during spraying. The melted particles hit the substrate, spread, and coalesce within each other to form a coating (Ref 28). The main advantage of flame spraying is that the melting and the consolidation of the polymer happen almost simultaneously during a single-step spraying process. Consequently, additional post-treatments are not necessary after the material deposition for the coating consolidation, such as post-curing at room temperature, ultraviolet radiation, or oven treatment, which are needed in some other surface technologies (Ref 9, 12). However, the temperature of the flame in thermal spraying is much higher than the melting temperature of polymers (Ref 29). Although specific equipment is available for flame spraying of polymers, a certain degree of material degradation always takes place during the flame processes (Ref 29). Therefore, fine tailoring of the process parameters is necessary to avoid the thermal degradation of the material, consisting of polymer chain scission, oxidation, surface embrittlement (Ref 30), and decrease in mechanical properties (Ref 29).

Our previous studies (Ref 31, 32) have demonstrated the icephobic property of thermally sprayed polymer coatings. For instance, polyethylene coatings showed potential icephobicity with ice adhesion value of 54 kPa for the polished surface (69 kPa for the as-sprayed surface). In addition, good coating durability was achieved for high-velocity impact test and particle erosion tests (Ref 31). Moreover, lubricant-infused porous coating (slippery liquid impregnated porous surface, SLIPS) showed extremely low ice adhesion (21 kPa for Thermally Sprayed SLIPS) and enhanced water repellency (Ref 32). However, further research is needed to optimise the manufacturing process of thermally sprayed icephobic coatings. Therefore, investigations are necessary on the effect of flame spraying parameters on the icephobicity of the surface. In particular, the process parameters strongly influence the performance of the coating (Ref 33). In addition, we have noticed that the chemical and thermal characterisations of the polymer coatings are essential in order to optimise the spray process for the selected purposes and coating requirements. Therefore, this study aims the optimisation of the process parameters to obtain an icephobic coating with preserved mechanical and structural properties. The influence of the process parameters on the coating properties was investigated by varying transverse speed and spraying distance of the spray gun for the polyethylene material. These parameters affect the heat input on the material during the process and thus the coating properties and its possible thermal degradation. In addition, the relationship between the icephobicity and the degradation of the coating is investigated, referring to the chemical and thermal characteristics of the flame-sprayed polymer coatings.

## Materials and Methods

### Material and Coating Fabrication

The material used in this work was a low-density polyethylene (LDPE) powder (Plascoat Europe BV, Zuidland, The Netherlands). The morphology of the polymer powder was analysed by a scanning electron microscope (SEM, Philips XL30, The Netherlands). The size distribution of the powder was below 300 μm for 95% of the particles, as given by the powder supplier. In addition, the particle size distribution was investigated by laser diffraction analysis using the dry powder method (LS 13 320 Laser Diffraction Particle Size Analyser, Beckman Coulter, Inc., United States). The coatings were prepared by using an oxygen-acetylene flame spray gun (CastoDyn DS 8000, Castolin Eutectic, Switzerland) with gas pressure for oxygen and acetylene of 4.2 bar and 0.7 bar, respectively. A powder feeder (Sulzer Metco 4MP, Oerlikon Metco, Switzerland) was used with compressed air as the carrier gas for feeding the powder in the gun. A powder feed rate of 26 g/min was defined for coating production. The coatings were automatically sprayed by a single-arm robot (ABB IRB 4400/60, ABB Robotics, Sweden), controlling the transverse speed and the spraying distance of the spray gun during the coating production. These two parameters were varied for the production of the polyethylene coatings,

keeping as constant all the others. In particular, the heat input of the combustion flame on the sprayed surface changed based on the combination of the chosen process parameters. In fact, the closer the spraying distance and the slower the transverse speed, the higher the heat transferred to the polymeric material. Consequently, a systematic study was designed to investigate the effect of the heat input of the process on the coating performances. The values of transverse speed and spraying distance and the number of specimens analysed in this work are summarised in Fig. 1. These values were chosen based on the parameters suggested by the spray gun manufacturer for spraying polymers. In particular, it was recommended to use a minimum spraying distance of 250 mm during the process production. However, we decided to spray only one sample by using 200-mm distance to investigate the effect of the heat input for an extreme condition of the chosen process window (sample A0). The coatings were sprayed on grit-blasted (alumina grits, 54 Mesh) stainless steel substrate (UNS S31603) with dimensions of 200 mm × 50 mm × 1.5 mm. Each coating was sprayed following fixed production steps, such as pre-heating of the substrate, spraying, and post-heating by flame. In particular, prior to the spraying, the substrates were pre-heated with the flame, to ensure good coating adhesion. After pre-heating, three layers of powder were sprayed with 5-mm step on the whole substrate to obtain a thick coating. A thermal imaging camera (Ti300 Infrared Camera IR Fusion Technology, Fluke Corporation, United States) was used to monitor the temperature of the metal substrate before spraying. The thermal camera was calibrated by experimentally measuring the emissivity of the substrate material. Then, the spraying of the coating started when the substrate reached the melting transition temperature of the polymer powder (around 120 °C). This monitoring avoided the over-melting of the substrate, which might cause the vaporisation of the polymer powder hitting the substrate. Moreover, this prevents the formation of defects in the polymer coating, such as voids, contaminants, and degradation (Ref 34). However, the monitored temperature was representative of the substrate until the spraying of the coating started. This is due to the different emissivities between the stainless steel substrate and polymer coating.

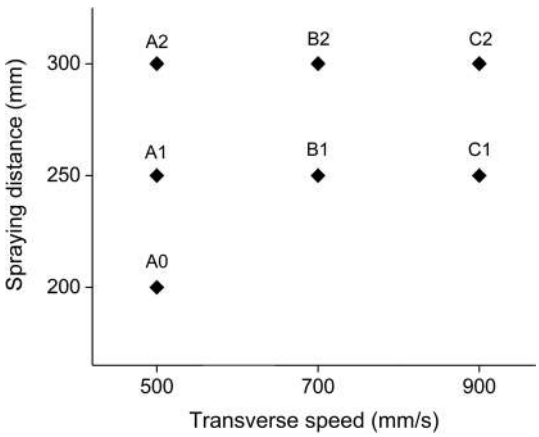


**Fig. 1** Process window of the chosen parameters for flame spraying of LDPE coatings. Samples were identified with letters (from A to C for increasing transverse speed) and with numbers (from 0 to 2 for increasing spraying distance)

## Microstructural and Surface Characterisation

The microstructure of the coating was analysed by a scanning electron microscope (SEM, Jeol, IT-500, Japan), investigating the presence of defects within the coating structure, such as voids and contaminations. In addition, energy dispersive x-ray spectroscopy (SEM/EDS) was used to obtain a semi-quantitative elemental composition (oxygen and carbon mass percentage, in the case of our material) in very specific locations of the cross section for coatings sprayed with different process parameters. For this test, the cross sections of the sample were coated by both carbon and gold sputtering to enhance the surface conductivity. The analysis was carried out by using an acceleration voltage of 10 kV in high vacuum by using a back-scattered electrons detector. This permitted the analysis of the coating chemical composition for different process parameters. Moreover, an optical microscope (Leica DM2500 M, Germany) was used to measure the thickness of the coating as an average of nine measurements in different points along the width of the specimen. The areal roughness (*Sa*) was measured with an optical profilometer (Alicona Infinite Focus G5, Alicona Imaging GmbH, Austria) by using 20× objective magnification in the areas of 2 × 2 $mm^2$, according to ISO 4288 procedure. The texture of the surface was analysed by using 5× objective magnification in areas of approximately 30 × 30 $mm^2$.

## Ice Accretion and Ice Adhesion

Ice adhesion test of the coatings was performed using the icing facilities at Tampere University (Ref 35). Firstly, artificial ice was accreted from supercooled droplets in the icing wind tunnel on a surface area of 30 × 30 $mm^2$ of the specimen. In the present and previous studies (Ref 31, 32, 35), a mixed-glaze type of ice was accreted onto the specimen surface. The characteristic icing parameters are summarised in Table 1. After the ice was formed, the ice adhesion was measured using the centrifugal ice adhesion test (CAT) in sub-zero ambient condition. In this method, the iced specimen is rotated with increasing speed until the ice detaches from the surface of the specimen. A sensor monitors the moment at which the ice detaches from the surface, and therefore, the ice adhesion can be evaluated. The test setup is described in detail in the previous work (Ref 35).

**Table 1** Parameters of the icing wind tunnel

| *Parameter* | |
|---|---|
| Room temperature | − 10 °C |
| Relative humidity | 83-86% |
| Water temperature | 6-7 °C |
| Air pressure | 3.5-4 bar |
| Airflow | 60-70 l/min |
| Water pressure | 3.5-4 bar |
| Water flow | 0.15-0.2 l/min |

The shear ice adhesion strength is evaluated as the ratio between the centrifugal force, $F$(N), at the moment of ice detachment and the iced area, $A(m^2)$, of the specimen. Equation 1 evaluates the adhesion strength, $\tau_{ice}$(kPa), as follows:

$$\tau_{ice} = \frac{F}{A} = \frac{m_{ice} r \omega^2}{A} \quad \text{(Eq 1)}$$

where $m_{ice}$(kg) is the mass of the accreted ice on the surface of the specimen, $r$(m) is the radial spinning length, and $\omega$(rad/s) is the rotational speed. The ice adhesion of the coating was evaluated as an average of four parallel samples during the icing accretion event. A test reference surface (TT) (Teflon tape, 3 M, United States) was tested to control the value of the ice adhesion for every accretion event. The reference material is essential to ensure the repeatability of the results, due to the variability of the ice adhesion strength for different icing conditions (Ref 36-38).

## Wettability

The wettability of the surfaces was examined using a droplet shape analyser (DSA100, Krüss, Germany) to evaluate the static contact angle and the roll-off angle of the water droplets on the coating surface. The experiments were performed by pouring 6 µl water droplets of ultra-high purity water (MilliQ, Millipore Corporation, United States) onto the surfaces. The tendency of the water droplet to roll off from the surface was investigated by tilting experiment. In particular, the angle of inclination of the sample was measured when the droplet rolled off from the coating surface. The values were evaluated as an average of five measurements in different areas of the same coating surface at 21 °C and 60% relative humidity.

## Chemical and Thermal Characterisations

Polymers are well-known heat-sensitive materials, and consequently, their structure is strongly influenced by the temperature reached by the material during flame spraying. This is mainly related to the time that the material spends in contact with the flame. In fact, the heat input of the process increases as the transverse speed and the spraying distance decreases (longer time process), producing possible oxidation and physical degradation of the sprayed polymer (Ref 34). For this reason, a thermal-processing window is recommended for each polymer to prevent excessive thermal degradation and consequently to ensure the quality of the coating. Therefore, chemical and thermal analyses of both the feedstock material and the coating were performed to analyse the possible thermal degradation produced by the process parameters, influencing the performance of the coating.

### *Fourier-Transform Infrared Spectroscopy (FTIR)*

The chemical characterisation of the polymer powder and the variation in the chemical structure of the coatings were investigated by using Fourier-transform infrared spectroscopy (FTIR) (Bruker Tensor 27 FT-IR spectrometer, Bruker, Sweden). The FTIR spectra were measured at room temperature using an attenuated total reflection (ATR) spectrometer whereas the internal reflection element (IRE) was a diamond crystal. The degree of polymer oxidation was determined by monitoring the change in intensity of non-volatile carbonyl oxidation products. The intensity of the absorbance peak at 1713 $cm^{-1}$ was taken as a measure of the concentration of carbonyl compounds derived by the polyethylene degradation (mainly carboxylic acids) (Ref 39, 40). All measurements were performed by using three samples taken from every coating surface.

### *Thermogravimetric Analysis (TGA)*

The variations in the thermal stability of the coating within the spraying-process window were investigated by thermogravimetric analysis (TGA) (Netzsch TGA209F Tarsus, Netzsch, Germany). The specimen weight was approximately 10 mg and a dynamical heating was performed at 20 °C/min from 25 to 600 °C in nitrogen atmosphere. Firstly, the degradation temperature of the polymer powder was measured at the maximum deflection point of the TG curve. Secondly, the thermal stability of the coatings and their degradation degree were evaluated by comparing the temperatures at which the 2% ($T_{98\%}$), the 5% ($T_{95\%}$), and the 10% ($T_{90\%}$) of the mass of the coating were lost during the thermal heating (Ref 41). In particular, the lower these temperatures, the higher the degree of degradation of the polymer coating during flame spraying.

### *Differential Scanning Calorimetry (DSC)*

The thermal characterisation of the powder and the influence of the process parameters on the degree of crystallinity of the coatings were evaluated by using a

differential scanning calorimetry (DSC) (Netzsch DSC214 Polyma, Netzsch, Germany). Test specimens were weighed approximately 10 mg. First dynamical heating was performed at 20 °C/min from − 20 to 150 °C in nitrogen atmosphere in order to evaluate the degree of crystallinity of the produced coating. In addition to this, to evaluate the maximum degree of crystallinity of the powder, a slow cooling at 1 °C/min was performed after the first heating to remove the effect of the thermal history due to the production process of the powder. Then, the second dynamic heating was carried out with parameters identical to the first heating only for the powder. The degree of crystallinity of the powder was compared to one of the coatings to understand the effect of the process parameters on the degree of crystallinity of the material after flame spraying. The degree of crystallinity $\chi$ was derived by the ratio of the measured heat of fusion and the heat of fusion for finite crystals for the considered polymer, as shown in Eq 2:

$$\chi = \frac{\Delta H}{\Delta H_{100\%}} \quad \text{(Eq 2)}$$

where $\Delta H$ (J/g) represents the melting enthalpy of the specimen (corresponding to the melting-peak area) and $\Delta H_{100\%}$ (J/g) represents the measured enthalpy based upon a perfect crystal heat of fusion of 293 J/g (Ref 42).

## Results and Discussion

Thermal spray technology, and especially flame spraying, represents a fast technique for the production of thermoplastic polymer coatings due to the advantage of the melting-consolidation transition of the polymer in one-step process. However, polymers are known to be heat-sensitive materials, and therefore, a thorough study is necessary to evaluate in detail the influence of the process parameters on the coating properties, such as thermal properties, mechanical performance, and durability. Moreover, the spray process parameters can influence the areal roughness of the coating, which has been considered as one of the main factors affecting the icephobicity of the surface (Ref 43, 44). For this reason, a compromise should be reached between the coating performances and the resulting surface properties affecting icephobicity, when selecting the process parameters.

### Powder Properties

The morphological analysis of the powder showed the presence of the different dimensions and shapes of the polymer particles. The powder morphology is shown in Fig. 2. In particular, the particle shape varied from small grain to stretched and narrowed flakes due to the method used for the powder production. The analysis of the powder dimensions indicated that 90% of the total particles count has a diameter smaller than 278 µm and that 10% of the total particles count is smaller than 104 µm. Moreover, the thermal characterisation of the powder was carried out to define the processing temperature of the coating. The LDPE powder showed a melting-peak temperature of 109 °C and a thermal degradation temperature of 427 °C (measured at the 2% mass loss of the TG curve of the LDPE powder, as it is indicated in Fig. 9). Table 2 summaries the LDPE powder properties.

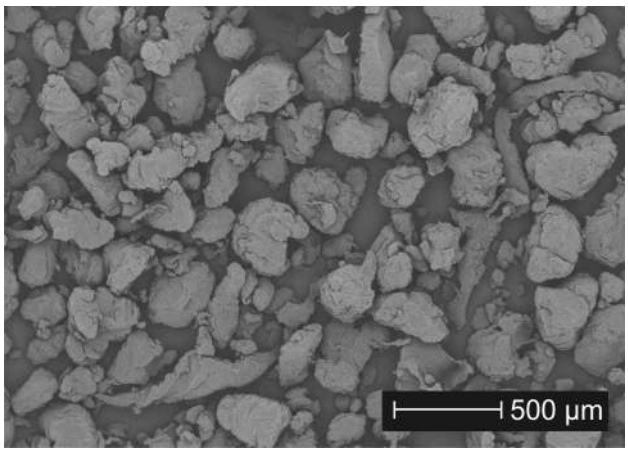


**Fig. 2** SEM image of LDPE powder

**Table 2** Properties of LDPE powder

| *Powder properties* | |
|---|---|
| Particle size distribution | − 278 + 104 µm |
| Peak melting, $T$ | 109 °C |
| Degradation, $T$ | 427 °C |

### Microstructural and Surface Properties of the Coatings

The microscopic analyses of the coatings revealed no defects within the structure, such as voids, even for the specimen that was visibly degraded using the spraying distance of 200 mm and the transverse speed 500 mm/s (sample A0), as shown in Fig. 3. The variation in coating thicknesses can be clearly visible from the cross sections of the coatings sprayed by using different parameters. In fact, the process parameters affected the deposition efficiency of the polymer powder, as we can see from the results of the thickness measurements in Fig. 4. Considering the powder-feeding rate and the spraying distance as constant, the thickness of the coating decreased as the transverse speed increased from 500 to 900 mm/s (A1, B1, C1 and A2, B2, C2 in Fig. 4). This result is reasonable if we assume that

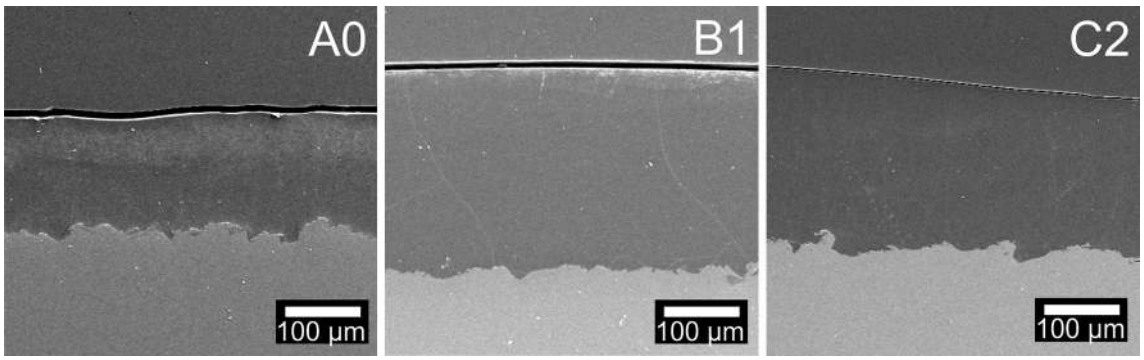


**Fig. 3** SEM images of the cross sections of LDPE coatings sprayed with different process parameters. In particular from left to right: A0 with 200 mm and 500 mm/s; B1 with 250 mm and 700 mm/s; C1 with 300 mm and 900 mm/s

the amount of material deposited per unit length decreases as the transverse speed increases during the spraying process (powder-feeding rate and spraying distance as constant). However, for heat-sensitive material, this fact is not obvious, due to the strong dependence of the flow properties of the polymer from the process temperature and the effect of the combustion flame on the polymer powder (Ref 33). In fact, for the specimens sprayed at 500 mm/s, we can see that the coating thickness is influenced by the heat input within the material produced by lower transverse speed (see A0, A1, A2 in Fig. 4).

The standard deviations of the thickness measurements increased as the transverse speed increased from 500 to 900 mm/s. This is due to the variability in the coating texture, being rougher for samples produced with the higher transverse speed. This result was confirmed by the optical profilometer analyses of the coating surface. These analyses showed a gradual increase in the areal roughness with increasing transverse speed. The resulting areal roughness was related to the chosen process parameters and varied from 5 µm for the sample A0 to 18 µm for the sample C2. Figure 5 summarises the surface texture images and the areal roughness values for all of the specimens analysed in this study.

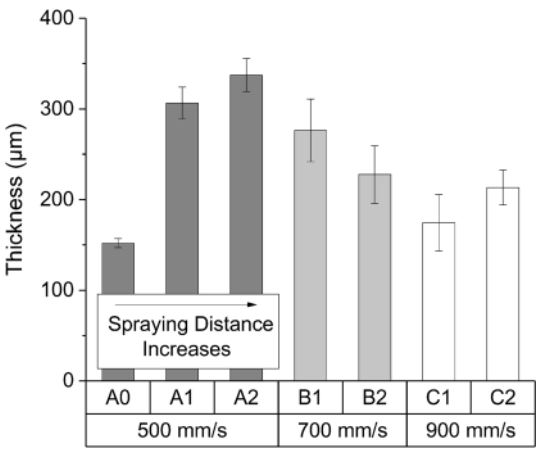


**Fig. 4** Thicknesses measurement from the cross-sectional images of the coatings

## Icephobicity and Wettability of the Coating Surface

A coating is considered icephobic when the adhesion of the ice formed on its surface is low enough that this can be easily removed by shear. However, different methods are used to evaluate the icephobicity of the surface. In particular, this can be evaluated by measuring the ice adhesion with different tests (Ref 45, 46), by studying the delay of droplet freezing (Ref 47, 48), the frost formation (Ref 49, 50), and the attitude of a cold surface to repel impacting water droplets (Ref 11, 51). In this work, the ice adhesion was measured by using the centrifugal adhesion method (Ref 35) to compare the icephobic characteristic of the produced coatings. For this test method, we defined a surface with low ice adhesion when the adhesion of ice is below 50 kPa (Ref 52). Moreover, the surface shows extremely low ice adhesion when the ice is shed off with a force lower than 10 kPa (Ref 52). Figure 6 represents the ice adhesion value (and standard deviation) and the areal roughness of the as-sprayed coatings.

The results showed a strong influence of the process parameters on the icephobicity of the coating surfaces. Firstly, for the slowest transverse speed (from A0 to A2), ice adhesions represented the highest values obtained in this study. The ice adhesion decreased with decreasing areal roughness according to the previous research (Ref 37, 53, 54). In particular, samples A resulted in the highest ice adhesion here, despite they represented the smoothest surfaces in comparison with the other coatings. This indicates that other factors are affecting the icephobicity of the surface in addition to areal roughness. Secondly, with the medium transverse speed (B1 and B2), no clear relation was found between the ice adhesion and the areal roughness. Thirdly, the lowest ice adhesion is reached with the specimen C1 ($32 \pm 3$ kPa), showing an optimal combination of parameters in the process window of this study.

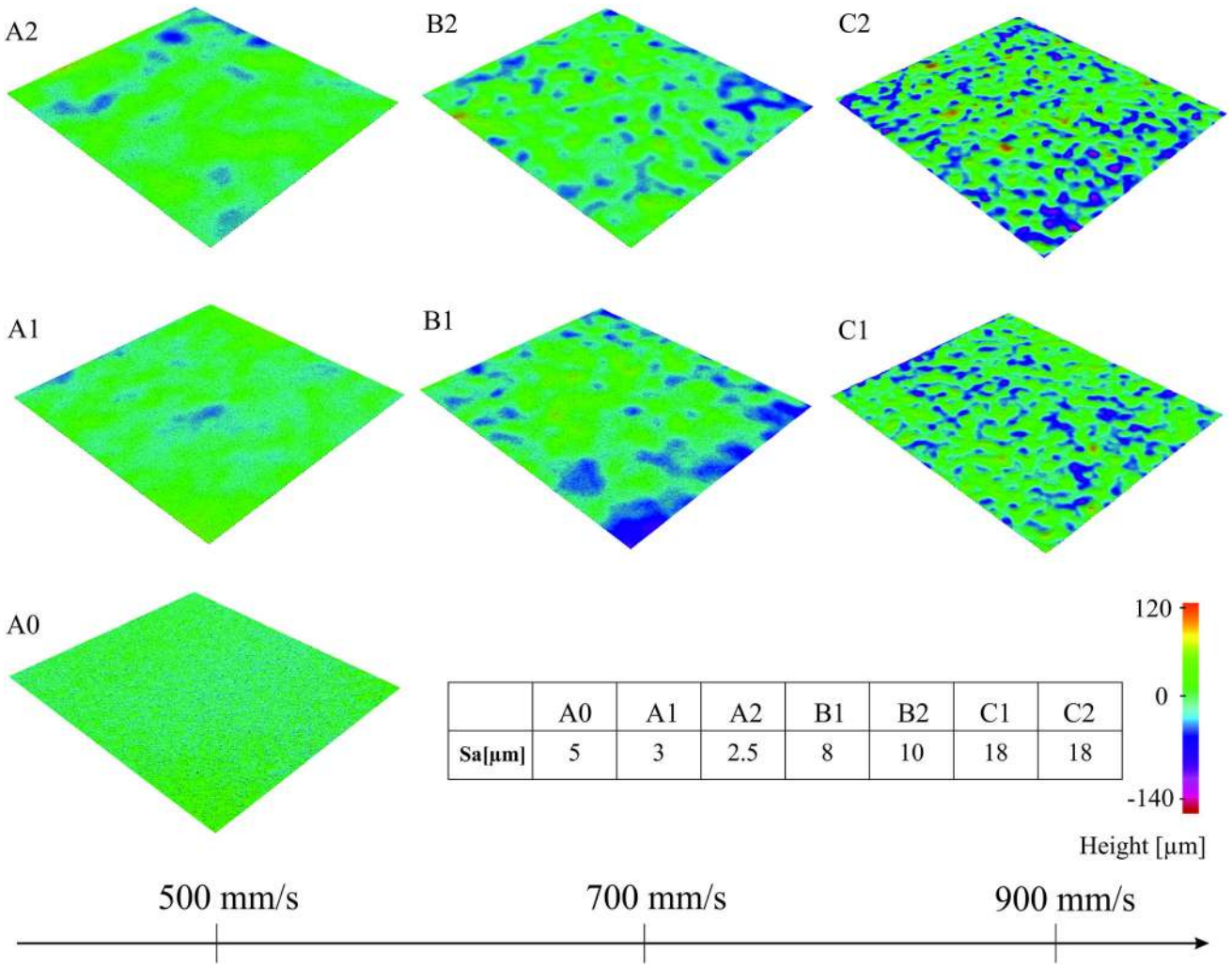


| | A0 | A1 | A2 | B1 | B2 | C1 | C2 |
|---|---|---|---|---|---|---|---|
| Sa[µm] | 5 | 3 | 2.5 | 8 | 10 | 18 | 18 |

**Fig. 5** Surface texture and areal roughness (Sa) of the coatings measured by optical profilometre analysis. The surface textures correspond to coating areas of approximately 30 × 30 mm$^2$

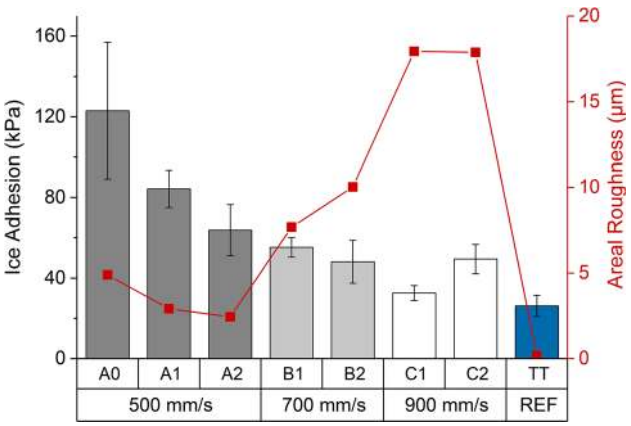


**Fig. 6** Ice adhesion (left axis) and areal roughness Sa (right axis) of the coatings. Teflon tape (TT) represents the reference material for ice adhesion used in this centrifugal test

The wettability of the surface represents another important property in the analysis of the icephobicity of the coatings. In previous studies, the wettability of the surface has shown to be beneficial for the icephobicity of surfaces (Ref 46). The hydrophobicity (water contact angle greater than 90°) or the superhydrophobicity (water contact angle greater than 150°) of the surface would prevent water droplets to strongly adhere to the surface before freezing occurs (Ref 55). The increased water contact angle and the decreased roll-off angle have shown a reduced ice adhesion for superhydrophobic coating when ice is frozen onto the surface (Ref 56). However, when the ice is accreted from supercooled droplets, no clear connection has been found between the ice adhesion and the wettability properties of the surface (Ref 52). The wettability properties of the polyethylene coatings analysed in this work are

**Table 3** The wettability properties of the polyethylene coatings

| Sample | Water contact angle, ° | Water roll-off angle, ° |
|---|---|---|
| A0 | 93(± 1) | > 90 |
| A1 | 90(± 1) | > 90 |
| A2 | 94(± 1) | > 90 |
| B1 | 93(± 1) | > 90 |
| B2 | 93(± 3) | > 90 |
| C1 | 89(± 2) | > 90 |
| C2 | 92(± 3) | > 90 |

summarised in Table 3. The water contact angle for the produced coatings varied from 89° to 94°, showing a general hydrophobic character of the surface. Moreover, all the surfaces showed a roll-off angle higher than 90°, with the water droplets pinned onto the surface; hence, no roll off was observed. No relation between the wettability and icephobicity of the surface was found for all the coatings on which impact ice was accreted. Consequently, we can conclude that the process parameters did not strongly affect the wettability of the produced surfaces, although their icephobicity varied. Considering the trend of the ice adhesion results in Fig. 6, one of the factors influencing the icephobicity of the coating can be related to the different heat inputs of the process on the polymer material. In the case of heat-sensitive polymers, thermal degradation plays an important role in the coating process due to the presence of the combustion flame (Ref 33). In fact, thermal degradation might cause crosslinking of the polymer chains, chain scission, oxidation, and loss in the molecular weight (Ref 34). Moreover, degradation produces the embrittlement of the polymer surface that visually shows the presence of surface micro-cracks. These promote the formation of mechanical interlocking between ice and the damaged coating surface, increasing the ice adhesion strength (Ref 57). In addition, the chemical structure of the surface influences on the icephobicity. The possible chemical modification of the coating during the flame spray process might play a role in the variation in the ice adhesion strength with the process parameters. These factors affecting icephobicity will be investigated by using chemical and thermal analyses.

## Chemical and Thermal Properties

In flame spraying, the combustion flame melts the polymer powder and the coating is formed by the molten particles hitting into the substrate surface (Ref 28). However, this flame causes the degradation of the polymer powder, especially for the smallest powder particles that do not withstand the flame temperature (they produce "sparks" in the flame). Moreover, the slowest transverse speed increases the time of the process, increasing the coating temperature (Ref 33). Consequently, degradation occurs by the mechanism of chain scission (producing short polymer chains and decreasing the molecular weight) and oxidation (Ref 29, 30, 58). The oxidation of thermally sprayed material is temperature and time-dependent process (Ref 28, 29, 59). The greater the time of exposition of the polymeric material to the flame, the higher the effect of the thermal oxidation in the deposited material. Two types of oxidation processes can be distinguished during the thermal spray process. Firstly, the oxidation process of the polymer powder occurs during the spraying of the powder passing the flame, known as in-flight oxidation. Secondly, the oxidation of the polymer splats, already deposited on the substrate, can happen during the coating formation. However, different researchers underlined the fundamental difficulty of separating the effect of these two stages of oxidation (Ref 28). The substrate temperature increases with increasing process time and decreased spraying distance (Ref 29, 60). For this reason, the chemical and thermal characterisations were needed for the flame-sprayed coatings to avoid the damage of mechanical properties, such as toughness and strength, and embrittlement of the coating surface (Ref 33).

The chemical analysis of the surfaces was carried out by investigating the possible variation in the FTIR spectra obtained for the different coatings in comparison with the virgin powder. Figure 7 represents the FTIR spectra of the powder (black curve) together with selected coating samples (AO, A1, A2, and C2). The FTIR spectrum of the LDPE powder (black curve in Fig. 7) showed the presence of the typical methylene peaks of the polyethylene polymer. In addition, the powder probably incorporates a conventional thermal stabiliser of an undisclosed composition containing polar (-OH) and carbonyl products (peak at 1734 $cm^{-1}$) (Ref 61). The main difference between the powder and the coatings spectra relied on the development of absorbance bands in the regions 1700-1750 $cm^{-1}$ and 800-1300 $cm^{-1}$, respectively. In addition, the presence of a new absorbance peak at 1713 $cm^{-1}$ was really evident for some of the sprayed coatings (intensity of absorbance peak at 1713 $cm^{-1}$ of 0.04 for the virgin powder). Specifically, the intensity of the absorbance peak at 1713 $cm^{-1}$ increased from 0.15 for the sample A2 to 0.30 for the sample A0, considering the coatings sprayed with the transverse speed of 500 mm/s. This increase in peak intensity indicated the greater modification of the chemical structure of the polyethylene with decreasing spraying distance during flame spraying. In particular, this new peak was related to the primary oxidation product formed by the thermal oxidation of polyethylene, mainly consisting of carboxylic acids and carbonyl compounds (Ref 40). In this research, oxygen is present both in the spraying

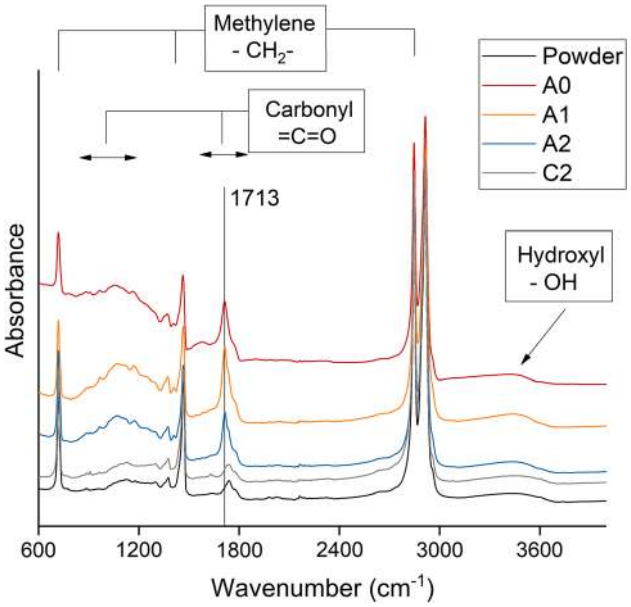


**Fig. 7** FTIR spectra of LDPE powder and flame-sprayed LDPE coating sprayed with 500 mm/s (A0, A1, A2) and with 900 mm/s (C2)

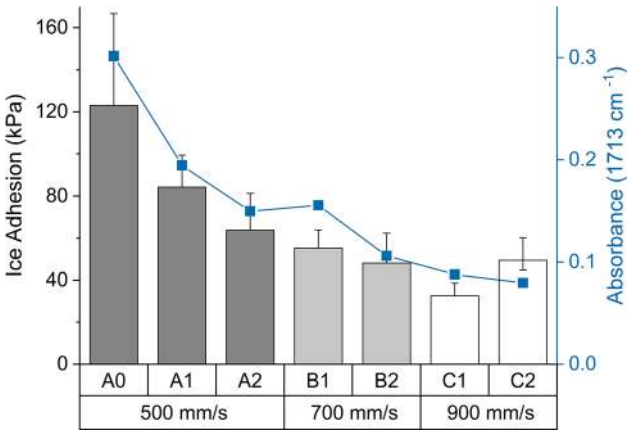


**Fig. 8** Ice adhesion strength and absorbance intensity at 1713 $cm^{-1}$ for the flame-sprayed LDPE coatings

environment and in the gas mixture used for the production of LDPE coatings. The principal chemical reactions of the oxidation mechanism of polyethylene can be described by three main stages (Ref 62). Firstly, free carbon radicals are produced from the polyethylene polymer chain via chain scission. The reaction is thermally initiated by the energy available from the combustion flame. Secondly, the oxygen reacts with the free carbon radicals to form peroxyl radicals, carbonyl compounds, and additional free carbon radicals. Finally, the free radicals react between each other to form carbonyl product, shorter polymer chain, and oxygen molecules (Ref 40, 62). The enhanced presence of the carbonyl products in the chemical structure confirmed that the thermal degradation of polyethylene gradually occurred at the coating surface as the heat input of the process increased. However, the production of carbonyl products gradually decreased as the combustion flame was further away from the coating surface and the time of the process was reduced. In particular, the specimen C2 (Fig. 7) revealed an FTIR spectrum similar to the polymer powder spectrum (the absorbance intensity at 1713 $cm^{-1}$ equal to 0.07) with no evidence of the peak at 1713 $cm^{-1}$. This verified that the process parameters strongly affect the chemical composition of the coating and consequently its icephobicity. Figure 8 shows the relationship between the absorbance intensity of the peak at 1713 $cm^{-1}$ for the produced coatings and the ice adhesion. We can see that the lower the intensity of the absorbance peak at 1713 $cm^{-1}$, the higher the icephobic behaviour of the coating. However, this trend was not verified for the sample C2 sprayed with 900 mm/s and 300 mm, where the degree of degradation was strongly decreased due to reduced process heat input for this combination of parameters (intensity equal to 0.07 for C2 and no evident peak at 1713 $cm^{-1}$ in Fig. 7).

To compare the effect of process parameters on polymer degradation, the time the polymer is exposed to elevated temperatures was approximately estimated. The time of exposition of the in-flight particles to the flame can be considered of the same order for every produced coating, as the polymer particles passed through the same combustion flame with the same velocity. Therefore, the main effect of degradation would directly depend on the oxidation of the polymer splats on the substrate during the coating deposition. This oxidation mainly depends on the combination of process parameters chosen for the coating production, such as the transverse speed and the spraying distance. The transverse speed mostly influences the duration of the process and the spraying distance mainly controls the temperature reached by the substrate during the process. For a chosen spraying distance, the lower the transverse speed, the higher the degree of thermal oxidation experienced by the coating (see absorbance value between A1, B1, C1 and A2, B2, C2 in Fig. 8). Moreover, for a chosen transverse speed, the lower the spraying distance, the higher the temperature reached by the substrate, the higher the degree of oxidation of LPDE coatings (see absorbance value between A0, A1, A2 and B1, B2 in Fig. 8). Previously, FTIR analysis verified the increase in carbonyl and carboxyl compounds (containing oxygen element) limited at the coating surface for different spraying parameters. To support this, the energy dispersive x-ray spectroscopy (SEM/EDS) was used to evaluate the possible presence of carbonyl compounds (containing oxygen) in the coating structure. The mass percentage of oxygen was measured to be $14 \pm 1$ and $8 \pm 0.5\%$ for samples A0 and C2,

respectively. These values corresponded to the average of three measurements analysed from the coating cross section. In particular, sample A0 showed a higher amount of oxygen in the coating structure, confirming the greater level of degradation produced during the process.

The thermogravimetric analysis (TGA) was used as an additional technique to investigate the thermal degradation of the coating. TGA represents a thermal analysis that reveals the temperature where the polymer can be processed without breaking down it into a gas. The FTIR results confirmed the formation of new carbonyl and carboxyl groups for the sprayed coating. This fact implied the chain scission of polyethylene and consequently the formation of short polymer chains (Ref 40, 62). These short chains will evaporate at a lower temperature than the longer polymer chain. Consequently, the higher the amount of short polymer chains within the coating structure, the lower the temperature measured for a certain percentage of mass loss. Based on this, the thermal stability of the coating was evaluated by comparing the temperatures at which the 2% ($T_{98\%}$), 5% ($T_{95\%}$), and 10% ($T_{90\%}$) of coating mass were lost during TGA test. The TGA curves of the virgin powder (black curve) and the sample A0 (red curve) are represented in Fig. 9. In addition, the temperature at 98, 95, and 90% of mass loss are indicated in the magnified part (grey rectangular area) of the TGA curves. The results from the thermogravimetric analysis are summarised in Table 4.

For all the test samples, no relevant mass loss was measured below 150 °C, confirming the absence of moisture within the material and ensuring that the evaluated mass loss was referring only to the polymer chain degradation. Firstly, the results showed a good initial thermal stability of the powder that could withstand the temperature of 427 °C by evaporating only 2% of its total mass. In fact, the higher the value of $T_{98\%}$, the greater the thermal stability of the coating. Secondly, this good thermal stability was generally reduced for all the produced coatings. Therefore, the stability was decreased for the A specimens, confirming the highest degree of degradation for the sample sprayed with the closer distance, A0. For medium transverse speed (B1), the thermal stability of the coating slightly improved in comparison with the coatings sprayed with 500 mm/s. Moreover, even lower degradation was revealed for the sample C2, showing the loss of mass of 2% around 417 °C. This behaviour was reproduced for all the coating, also if we consider the temperatures at 5% mass loss ($T_{95\%}$) and 10% mass loss ($T_{90\%}$) in Table 4. These results strongly confirmed the decrease in thermal stability of the coating with the increased heat input on the polymer during the process. In fact, with decreasing transverse speed and spraying distance, the substrate can heat-up for a longer period of time, producing thermal degradation of the coating.

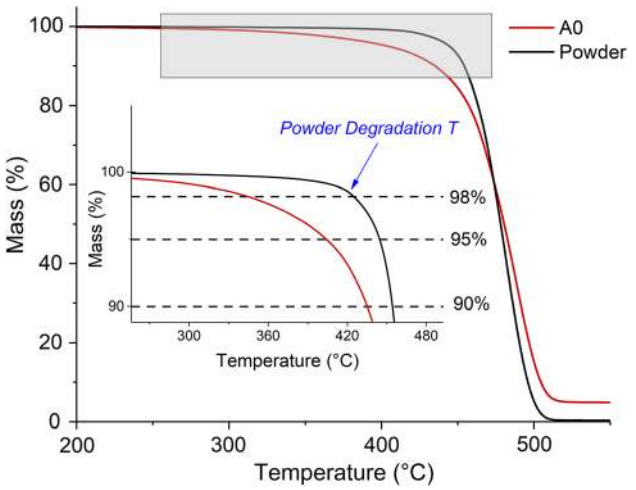


**Fig. 9** TGA curve of the virgin powder (black curve) and sample A0 (red curve). The magnified part of the graph represents the evaluation of the temperature corresponding to mass loss of 2, 5, and 10% (Color figure online)

**Table 4** Results of the thermogravimetric analysis

| Sample | $T_{98\%}$, °C | $T_{95\%}$, °C | $T_{90\%}$, °C |
|---|---|---|---|
| Powder | 427 | 444 | 454 |
| A0 | 350 | 404 | 435 |
| A1 | 363 | 408 | 434 |
| A2 | 370 | 415 | 434 |
| B1 | 380 | 424 | 443 |
| C2 | 417 | 438 | 451 |

The effect of the thermal history produced by the flame spray process on the degree of crystallinity of the coating was investigated by differential scanning calorimetry (DSC). The degree of crystallinity represents an important feature for semi-crystalline thermoplastic polymers, such as LDPE. In fact, this property is directly proportional to the mechanical properties of the coating, such as tensile strength and modulus (Ref 63), and to its barrier properties, such as moisture, solvent absorption, and oxygen permeation (Ref 64). For this reason, the degree of crystallinity of the coatings should be as close as possible to the one of the original powder, as an indication of reduced thermal degradation. Figure 10 represents the endothermic melting peaks of the LDPE polymer both for the powder (black curve) and the coatings sprayed with 500 and 900 mm/s.

The curves in Fig. 10 showed the broadening of the melting-peak transition and the decrease in the melting-peak intensity, gradually passing from the virgin powder (black curve) to the sample A0 (red curve). This effect was clearly related to the degradation process (mainly polymer chain scission) of the low-density polyethylene polymer, as

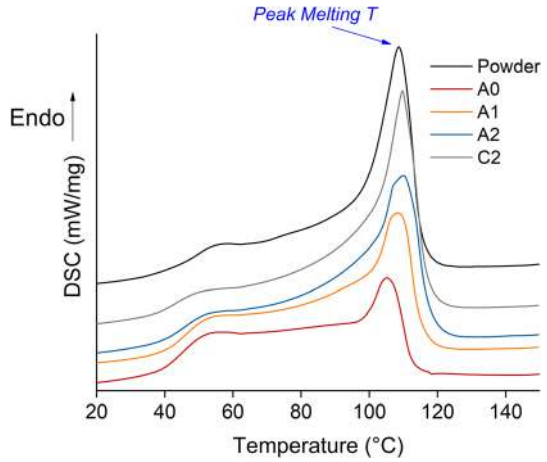


**Fig. 10** Melting transition of LDPE powder and flame-sprayed coatings with 500 mm/s (A0, A1, and A2) and 900 mm/s (C2)

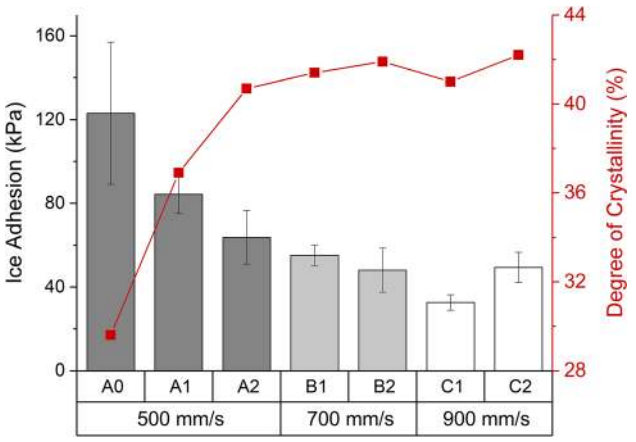


**Fig. 11** Relationship between the ice adhesion strength (left axis) and the degree of crystallinity (right axis) of flame-sprayed LDPE coatings

**Table 5** Melting temperatures and degree of crystallinity of LDPE powder and flame-sprayed coatings

| Sample | $\Delta H$, J/g | $T_m$, °C | $\chi$, % |
|---|---|---|---|
| Powder | 126.3 | 107.7 | 43 |
| A0 | 86.8 | 105.2 | 29 |
| A1 | 108.2 | 108.5 | 37 |
| A2 | 119.4 | 110.0 | 40 |
| B1 | 121.3 | 107.6 | 41 |
| B2 | 123.0 | 108.7 | 42 |
| C1 | 120.3 | 107.9 | 41 |
| C2 | 123.8 | 109.8 | 42 |

observed in the previous studies (Ref 65). No evident differences were found between the curve of the powder and sample C2, confirming the reduced thermal degradation. The melting temperature ($T_m$), the melting enthalpy ($\Delta H$), and the degree of crystallinity ($\chi$) were evaluated for the flame-sprayed coatings by analysing the first dynamical heating. These values are summarised in Table 5. The values of the powder referred to the second heating after a slow cooling in the test. In fact, the melting transition of the first heating of the powder is related to the thermal history that the polymer undergoes during its production process. Consequently, this is not representative of the degree of crystallinity of the virgin material. For this reason, a second heating after the slow cooling was performed to obtain the maximum degree of crystallinity of the virgin powder.

The degree of crystallinity for the LDPE powder after a slow cooling was evaluated as 43%. This value was in the typical range of crystallinity for LDPE polymer, evaluated by DSC (Ref 66). Moreover, the degree of crystallinity of the polymer gradually increased as the heat input of the process decreased (increased spraying distance from A0 to A2 in Table 5). This effect was reduced for samples C, showing decreased thermal degradation (FTIR graph in Fig. 7). In addition, as shown by the FTIR spectrum (Fig. 7), the gradual degradation of the coating probably generated radical reactions that caused the crosslinking of the LDPE and, in some cases, reduced its crystallinity (Ref 67). In this study, a clear correlation was found between the ice adhesion strength and the degree of crystallinity of the coating, as shown in Fig. 11.

The degree of crystallinity was strongly influenced by the heat input of the process for the samples A0, A1, and A2, increasing from 29 to 40%. A slightly further increase was revealed for samples B, and then, the degree of crystallinity was independent of the chosen process parameters for the coldest temperatures. We can generally conclude that the thermal degradation of the polymer negatively influenced its degree of crystallinity within the considered process window. Moreover, the variation in the degree of crystallinity due to thermal degradation strongly influenced the mechanical properties of the polyethylene, such as its tensile strength, ductility, stiffness, and toughness (Ref 62). In addition, the barrier properties of the coating, such as permeability to air and moisture, represent an important aspect in relation to the ice adhesion of the coating. The previous studies have shown that the permeability of thermally aged PE film increases for both moisture and air, showing a decrease in the barrier properties of the material (Ref 68). In fact, the higher permeability of water within the coating structure could be easily related to the tendency of supercooled droplets to penetrate the surface. However, these properties were not investigated in this study. Therefore, it cannot be excluded that they could be connected with the reduction in the icephobic behaviour of the surface with increasing thermal degradation. We can conclude that the thermal degradation of the polymer is

correlated with the icephobicity of the surface, showing the higher ice adhesion strength for the most degraded polymer surfaces. However, further investigations are necessary to evaluate which aspect of thermal degradation, such as chain scission, oxidation, or surface embrittlement, directly influences the surface icephobicity.

## Conclusions

In this study, icephobic LDPE coatings were produced with flame spraying by varying the heat input during coating processing. This was done by changing the transverse speed and the spraying distance of the spray gun. The optimisation of the parameters for the icephobic application was achieved through the process window designed for the LDPE coatings. In particular, it was found that the process parameters strongly affected the areal roughness of the coatings and the heat input during the production process. This increased the thermal degradation of the polymer coating, compromising its thermal stability, degree of crystallinity, and consequently its icephobic behaviour. For this reason, the heat input should be monitored during flame spraying of polymeric material to avoid the decrease in the coating properties. Here, we found that the most icephobic coating (ice adhesion strength 32 $\pm$ 3 kPa) was produced by using 900-mm/s transverse speed and 250-mm spraying distance. The areal roughness affected the ice adhesion, but no clear relationship was established for these samples. However, the thermal effect was shown to represent the main factor influencing the icephobicity of the coating. The heat input of the process influences both on the areal roughness and the thermal degradation of the coating. The higher the processing temperature of the polymer, the smoother the surface produced and the greater the material degradation. Connections were found between the thermal properties of the LDPE coating and the icephobic characteristic of the surface. In particular, an increase in the coating degradation (intensity of the absorbance peak at 1713 $cm^{-1}$) was strongly correlated with the decrease in the icephobicity for certain heat-input limit. After that, coatings achieve a relatively stable behaviour within the property deviation. Similarly, the degree of crystallinity increased as the degree of thermal degradation decreased and a good relationship was found with the decrease in ice adhesion until the limit. Moreover, this study showed that thermal stability is necessary for higher ice adhesion performance. This can be assumed to be one of the dominant factors in flame spraying of polymers. However, the coating degradation can be caused during both spraying and post-heating steps for these samples. Therefore, to understand better the effect of the process steps on the coating quality, further investigations will focus on their influence on the coating degradation and consequently on the icephobicity of the surface.

**Acknowledgments** Authors thank the LubISS (Lubricant Impregnated Slippery Surfaces) project that has received funding from the European Union's Horizon 2020 research and innovation programme under the Marie Sklodowska-Curie Grant Agreement No. 722497. Mr. Anssi Metsähonkala of Tampere University is acknowledged for operating the flame spray process, M.Sc. Jarmo Laakso of Tampere University for the SEM/EDS analysis, and M.Sc. Matteo Orlandini of Millidyne Oy for the particle size analysis. M.Sc. Henna Niemelä-Anttonen and B.Sc. Enni Hartikainen of Tampere University are thanked for assisting the ice accretion and the ice adhesion testing.



## References

1. M. Farzaneh, *Atmospheric Icing of Power Networks*, M. Farzaneh, Ed., Springer Science + Business Media B.V, New York, 2008, https://doi.org/10.1007/978-1-4020-8531-4
2. J.L. Laforte, M.A. Allaire, and J. Laflamme, State-of-the-Art on Power Line de-Icing, *Atmos. Res.*, 1998, **46**(1–2), p 143-158. https://doi.org/10.1016/s0169-8095(97)00057-4
3. F.T. Lynch and A. Khodadoust, Effects of Ice Accretions on Aircraft Aerodynamics, *Prog. Aerosp. Sci.*, 2001, **37**(8), p 669-767. https://doi.org/10.1016/S0376-0421(01)00018-5
4. X. Huang, N. Tepylo, V. Pommier-Budinger, M. Budinger, E. Bonaccurso, P. Villedieu, and L. Bennani, A Survey of Icephobic Coatings and Their Potential Use in a Hybrid Coating/Active Ice Protection System for Aerospace Applications, *Prog. Aerosp. Sci.*, 2019, **105**, p 74-97. https://doi.org/10.1016/j.paerosci.2019.01.002
5. O. Parent and A. Ilinca, Anti-Icing and de-Icing Techniques for Wind Turbines: Critical Review, *Cold Reg. Sci. Technol.*, 2011, **65**(1), p 88-96. https://doi.org/10.1016/j.coldregions.2010.01.005
6. G.D. Lunn, M.A. Riley, and D.G. McCartney, A Study of Wire Breakup and In-Flight Particle Behavior During Wire Flame Spraying of Aluminum, *J. Therm. Spray Technol.*, 2017, **26**(8), p 1947-1958. https://doi.org/10.1007/s11666-017-0639-1
7. J.-D. Brassard, C. Laforte, F. Guerin, and C. Blackburn, Icephobicity: Definition and Measurement Regarding Atmospheric Icing, *Adv. Polym. Sci.*, 2017, https://doi.org/10.1007/12_2017_36
8. Y. Wang, M. Li, T. Lv, Q. Wang, Q. Chen, and J. Ding, Influence of Different Chemical Modifications on the Icephobic Properties of Superhydrophobic Surfaces in a Condensate Environment, *J. Mater. Chem. A*, 2015, **3**(9), p 4967-4975. https://doi.org/10.1039/C4TA07077A
9. K. Golovin, S.P.R. Kobaku, D.H. Lee, E.T. DiLoreto, J.M. Mabry, and A. Tuteja, Designing Durable Icephobic Surfaces, *Sci. Adv.*, 2016, **2**(3), p e1501496. https://doi.org/10.1126/sciadv.1501496
10. M.J. Kreder, J. Alvarenga, P. Kim, and J. Aizenberg, Design of Anti-Icing Surfaces: Smooth, Textured or Slippery?, *Nat. Rev. Mater.*, 2016, **1**(1), p 15003

11. L. Cao, A.K. Jones, V.K. Sikka, J. Wu, and D. Gao, Anti-Icing Superhydrophobic Coatings, *Langmuir*, 2009, **25**(21), p 12444-12448. https://doi.org/10.1021/la902882b
12. Y.H. Yeong, A. Milionis, E. Loth, and J. Sokhey, Self-Lubricating Icephobic Elastomer Coating (SLIC) for Ultralow Ice Adhesion with Enhanced Durability, *Cold Reg. Sci. Technol.*, 2018, **148**, p 29-37. https://doi.org/10.1016/j.coldregions.2018.01.005
13. Q. Fu, X. Wu, D. Kumar, J.W.C. Ho, P.D. Kanhere, N. Srikanth, E. Liu, P. Wilson, and Z. Chen, Development of Sol–Gel Icephobic Coatings: Effect of Surface Roughness and Surface Energy, *ACS Appl. Mater. Interfaces.*, 2014, **6**(23), p 20685-20692. https://doi.org/10.1021/am504348x
14. D. Tejero-Martin, M. Rezvani Rad, A. McDonald, and T. Hussain, Beyond Traditional Coatings: A Review on Thermal-Sprayed Functional and Smart Coatings, *J. Therm. Spray Technol.*, 2019, **28**(4), p 598-644. https://doi.org/10.1007/s11666-019-00857-1
15. N. Espallargas, *Future Development of Thermal Spray Coatings: Types, Designs, Manufacture and Applications*, Elsevier, Cambridge, 2015, https://doi.org/10.1016/B978-0-85709-769-9.00006-3
16. F.Y. Yan, K.A. Gross, G.P. Simon, and C.C. Berndt, Mechanical and Erosion Properties of CaCO3-EMAA Thermal Sprayed Coatings, *Polym. Eng. Sci.*, 2004, **44**(8), p 1448-1459. https://doi.org/10.1002/pen.20141
17. C.C. Berndt, D. Otterson, M.L. Allan, C.C. Berndt, and D. Otterson, Polymer Coatings for Corrosion Protection in Biochemical Treatment of Geothermal Residues, *Geotherm. Resour. Counc. Trans.*, 1998, **22**, p 425-429
18. T. Sugama, R. Kawase, C.C. Berndt, and H. Herman, An Evaluation of Methacrylic Acid-Modified Poly(Ethylene) Coatings Applied by Flame Spray Technology, *Prog. Org. Coat.*, 1995, **25**(2), p 205-216. https://doi.org/10.1016/0300-9440(94)00507-W
19. X. Chen, J. Yuan, J. Huang, K. Ren, Y. Liu, S. Lu, and H. Li, Large-Scale Fabrication of Superhydrophobic Polyurethane/Nano-$Al_2O_3$ Coatings by Suspension Flame Spraying for Anti-Corrosion Applications, *Appl. Surf. Sci.*, 2014, **311**, p 864-869. https://doi.org/10.1016/j.apsusc.2014.05.186
20. R.A.X. Nunes, S. Wagner, and J.R.T. Branco, Atrito e Desgaste de Recobrimentos de PET, Politeraftalato de Etileno, Pós-Consumo Processados Por Aspersão Térmica (Friction and Wear of Polyethylene Terephthalate (PET) coating after consumption processed by thermal spraying), *Polímeros Ciência e Tecnol.*, 2007, **17**(3), p 244-249 ((In Portuguese))
21. C. Mateus, S. Costil, R. Bolot, and C. Coddet, Ceramic/Fluoropolymer Composite Coatings by Thermal Spraying—a Modification of Surface Properties, *Surf. Coat. Technol.*, 2005, **191**(1), p 108-118. https://doi.org/10.1016/j.surfcoat.2004.04.084
22. Y. Bao, D.T. Gawne, and T. Zhang, Effect of Feedstock Particle Size on the Heat Transfer Rates and Properties of Thermally Sprayed Polymer Coatings, *Trans. Inst. Met. Finish.*, 1995, **73**(pt 4), p 119-124
23. X. Chen, Y. Gong, X. Suo, J. Huang, Y. Liu, and H. Li, Construction of Mechanically Durable Superhydrophobic Surfaces by Thermal Spray Deposition and Further Surface Modification, *Appl. Surf. Sci.*, 2015, **356**, p 639-644. https://doi.org/10.1016/j.apsusc.2015.08.156
24. L.D. Stephenson, A.D. Beitelman, R.G. Lampo, A. Kumar, D. Neale, L. Clark, K. Palutke, M. Surratt, and D. Butler, Demonstration of Thermally Sprayed Metal and Polymer Coatings for Steel Structures at Fort Bragg, NC, No. ERDC/CERL TR-17-30, ERDC-CERL Champaign United States, 2017
25. P.J. Loustaunau and D. Horton, EMAA Thermoplastic Powder Coatings: Shop and Field Applications of Powder Coatings for Aggressive Environments, No. CONF.-94022-, NACE International, Houston, TX (United States), 1994. https://www.osti.gov/biblio/70079
26. Z. Jia, Y. Liu, Y. Wang, Y. Gong, P. Jin, X. Suo, and H. Li, Flame Spray Fabrication of Polyethylene-Cu Composite Coatings with Enwrapped Structures: A New Route for Constructing Antifouling Layers, *Surf. Coat. Technol.*, 2017, **309**, p 872-879. https://doi.org/10.1016/j.surfcoat.2016.10.071
27. M. Zhai, Y. Gong, X. Chen, T. Xiao, G. Zhang, L. Xu, and H. Li, Mass-Producible Hydrophobic per Fl Uoroalkoxy/Nano-Silver Coatings by Suspension Fl Ame Spraying for Antifouling and Drag Reduction Applications, *Surf. Coat. Technol.*, 2017, **328**, p 115-120. https://doi.org/10.1016/j.surfcoat.2017.08.049
28. L. Pawlowski, *The Science and Engineering of Thermal Spray Coatings*, 2nd ed., Wiley, Chichester, 2008, https://doi.org/10.1002/9780470754085
29. E. Petrovicova and L.S. Schadler, Thermal Spraying of Polymers, *Int. Mater. Rev.*, 2002, **47**(4), p 169-190. https://doi.org/10.1179/095066002225006566
30. J.A. Brogan, C.C. Berndt, G.P. Simon, and D. Hewitt, Physical and Relaxation Properties of Flame-Sprayed Ethylene-Methacrylic Acid Copolymer, *Polym. Eng. Sci.*, 1998, **38**(11), p 1873-1881
31. H. Koivuluoto, C. Stenroos, M. Kylmälahti, M. Apostol, J. Kiilakoski, and P. Vuoristo, Anti-Icing Behavior of Thermally Sprayed Polymer Coatings, *J. Therm. Spray Technol.*, 2017, **26**(1–2), p 150-160. https://doi.org/10.1007/s11666-016-0501-x
32. H. Niemelä-Anttonen, H. Koivuluoto, M. Kylmälahti, J. Laakso, and P. Vuoristo, Thermally Sprayed Slippery and Icephobic Surfaces, *ITSC2018-Proceedings of the International Thermal Spray Conference*, F. Azarmi, K. Balani, T. Eden, T. Hussain, Y.-C. Lau, H. Li, and K. Shinoda, Ed., ASM International, Orlando, 2018, p 380-384
33. T. Zhang, D.T. Gawne, and Y. Bao, The Influence of Process Parameters on the Degradation of Thermally Sprayed Polymer Coatings, *Surf. Coat. Technol.*, 1997, **96**, p 337-344. https://doi.org/10.1016/S0257-8972(97)00269-7
34. J.A. Brogan, Thermal-Spraying of Polymers and Polymer Blends, *MRS Bull.*, 2000, **25**(7), p 48-53. https://doi.org/10.1557/mrs2000.124
35. H. Koivuluoto, C. Stenroos, R. Ruohomaa, G. Bolelli, L. Lusvarghi, and P. Vuoristo, Research on Icing Behavior and Ice Adhesion Testing of Icephobic Surfaces, *Proceedings of* 16*th International Workshop on Atmospheric Icing of Structures-IWAIS XVI*, Jun 28–Jul 3, (Uppsala, Sweden), 2015, p 6
36. F. Guerin, C. Laforte, M.I. Farinas, and J. Perron, Analytical Model Based on Experimental Data of Centrifuge Ice Adhesion Tests with Different Substrates, *Cold Reg. Sci. Technol.*, 2016, **121**, p 93-99. https://doi.org/10.1016/j.coldregions.2015.10.011
37. S. Tarquini, C. Antonini, A. Amirfazli, M. Marengo, and J. Palacios, Investigation of Ice Shedding Properties of Superhydrophobic Coatings on Helicopter Blades, *Cold Reg. Sci. Technol.*, 2014, **100**, p 50-58. https://doi.org/10.1016/j.coldregions.2013.12.009
38. C. Stenroos, P. Vuoristo, and H. Koivuluoto, "Properties of Icephobic Surfaces in Different Icing Conditions," Master thesis, Tampere University Technology, Tampere, Finland, 2015
39. S. Therias, J.-L. Gardette, B. Pukánszky, T. Janecska, A. Perthue, M. Gardette, and E. Földes, Photo- and Thermal-Oxidation of Polyethylene: Comparison of Mechanisms and Influence of Unsaturation Content, *Polym. Degrad. Stab.*, 2013, **98**(11), p 2383-2390. https://doi.org/10.1016/j.polymdegradstab.2013.07.017
40. M. Sugimoto, A. Shimada, H. Kudoh, K. Tamura, and T. Seguchi, Product Analysis for Polyethylene Degradation by Radiation

and Thermal Ageing, *Radiat. Phys. Chem.*, 2013, **82**(1), p 69-73. https://doi.org/10.1016/j.radphyschem.2012.08.009
41. P. Gałka, J. Kowalonek, and H. Kaczmarek, Thermogravimetric Analysis of Thermal Stability of Poly(Methyl Methacrylate) Films Modified with Photoinitiators, *J. Therm. Anal. Calorim.*, 2014, **115**(2), p 1387-1394. https://doi.org/10.1007/s10973-013-3446-z
42. B. Wunderlich, *Thermal Analysis of Polymeric Materials*, Springer, Berlin, 2005, https://doi.org/10.1007/b137476
43. M. Zou, S. Beckford, R. Wei, C. Ellis, G. Hatton, and M.A. Miller, Effects of Surface Roughness and Energy on Ice Adhesion Strength, *Appl. Surf. Sci.*, 2011, **257**(8), p 3786-3792. https://doi.org/10.1016/j.apsusc.2010.11.149
44. M.F. Hassan, H.P. Lee, and S.P. Lim, The Variation of Ice Adhesion Strength with Substrate Surface Roughness, *Meas. Sci. Technol.*, 2010, **21**(7), p 75701-75709. https://doi.org/10.1088/0957-0233/21/7/075701
45. C. Laforte and J.-L.J. Laforte, Tensile, Torsional and Bending Strain at the Adhesive Rupture of an Iced Substrate, *Proceedings of the 28th International Conference on Ocean, Offshore and Arctic Engineering - OMAE* 2009, May 31–Jun 5, (Honolulu, Hawaii, USA), ASME, 2009, p 79–86
46. A.J. Meuler, J.D. Smith, K.K. Varanasi, J.M. Mabry, G.H. McKinley, and R.E. Cohen, Relationships between Water Wettability and Ice Adhesion, *ACS Appl. Mater. Interfaces.*, 2010, **2**(11), p 3100-3110. https://doi.org/10.1021/am1006035
47. P. Tourkine, M. Le Merrer, and D. Quéré, Delayed Freezing on Water Repellent Materials, *Langmuir*, 2009, **25**(13), p 7214-7216. https://doi.org/10.1021/la900929u
48. F. Arianpour, M. Farzaneh, and S.A. Kulinich, Hydrophobic and Ice-Retarding Properties of Doped Silicone Rubber Coatings, *Appl. Surf. Sci.*, 2013, **265**, p 546-552. https://doi.org/10.1016/j.apsusc.2012.11.042
49. P. Kim, T.S. Wong, J. Alvarenga, M.J. Kreder, W.E. Adorno-Martinez, and J. Aizenberg, Liquid-Infused Nanostructured Surfaces with Extreme Anti-Ice and Anti-Frost Performance, *ACS Nano*, 2012, **6**(8), p 6569-6577. https://doi.org/10.1021/nn302310q
50. A. Kirillova, L. Ionov, I.V. Roisman, and A. Synytska, Hybrid Hairy Janus Particles for Anti-Icing and De-Icing Surfaces: Synergism of Properties and Effects, *Chem. Mater.*, 2016, **28**(19), p 6995-7005. https://doi.org/10.1021/acs.chemmater.6b02765
51. K.K. Varanasi, T. Deng, J.D. Smith, M. Hsu, and N. Bhate, Frost Formation and Ice Adhesion on Superhydrophobic Surfaces, *Appl. Phys. Lett.*, 2010, **97**(90), p 234102. https://doi.org/10.1063/1.2731434
52. H. Niemelä-Anttonen, H. Koivuluoto, M. Tuominen, H. Teisala, P. Juuti, J. Haapanen, J. Harra, C. Stenroos, J. Lahti, J. Kuusipalo, J.M. Mäkelä, and P. Vuoristo, Icephobicity of Slippery Liquid Infused Porous Surfaces under Multiple Freeze-Thaw and Ice Accretion-Detachment Cycles, *Adv. Mater. Interfaces*, 2018, **5**(20), p 1800828. https://doi.org/10.1002/admi.201800828
53. R.J. Scavuzzo and M.L. Chu, *Structural Properties of Impact Ices Accreted on Aircraft Structures*, NASA Cr-179580, NASA-Lewis Research Centre, Cleveland, 1987
54. D.L. Loughborough and E.G. Hass, Reduction of the Adhesion of Ice to De-Icer Surfaces, *J. Aeronaut. Sci.*, 1946, **13**(3), p 126-134. https://doi.org/10.2514/8.11328
55. J. Chanda, L. Ionov, A. Kirillova, and A. Synytska, New Insight into Icing and De-Icing Properties of Hydrophobic and Hydrophilic Structured Surfaces Based on Core-Shell Particles, *Soft Matter*, 2015, **11**(47), p 9126-9134. https://doi.org/10.1039/c5sm02143j
56. Y. Shen, H. Tao, S. Chen, L. Zhu, T. Wang, and J. Tao, Icephobic/Anti-Icing Potential of Superhydrophobic Ti6Al4 V Surfaces with Hierarchical Textures, *RSC Adv.*, 2015, **5**(3), p 1666-1672. https://doi.org/10.1039/C4RA12150C
57. J. Chen, J. Liu, M. He, K. Li, D. Cui, Q. Zhang, X. Zeng, Y. Zhang, J. Wang, and Y. Song, Superhydrophobic Surfaces Cannot Reduce Ice Adhesion, *Appl. Phys. Lett.*, 2012, **101**(11), p 111603. https://doi.org/10.1063/1.4752436
58. F. Khabbaz, A.C. Albertsson, and S. Karlsson, Chemical and Morphological Changes of Environmentally Degradable Polyethylene Films Exposed to Thermo-Oxidation, *Polym. Degrad. Stab.*, 1999, **63**(1), p 127-138. https://doi.org/10.1016/S0141-3910(98)00082-2
59. R. Perrin and J.P. Scharff, *Chimie Industrielle*, 2nd ed., Industrial Chemistry, Masson, 1997 ((In French))
60. Y. Bao, D.T. Gawne, D. Vesely, and M.J. Bevis, Formation and Microstructure of Plasma Sprayed Polyamide Coatings, *Surf. Eng.*, 1994, **10**(4), p 307-313
61. A.C. Albertsson, C. Barenstedt, and S. Karlsson, Susceptibility of Enhanced Environmentally Degradable Polyethylene to Thermal and Photo-Oxidation, *Polym. Degrad. Stab.*, 1992, **37**(2), p 163-171. https://doi.org/10.1016/0141-3910(92)90080-O
62. B. Zhao, S. Zhang, C. Sun, J. Guo, Y.X. Yu, and T. Xu, Aging Behaviour and Properties Evaluation of High-Density Polyethylene (HDPE) in Heating-Oxygen Environment, *IOP Conf. Ser. Mater. Sci. Eng.*, 2018, **369**, p 012021. https://doi.org/10.1088/1757-899X/369/1/012021
63. R. Ferhoum, Analysis of Thermal Ageing Effect (Hold Time - Crystallinity Rate - Mechanical Property) on High Density Polyethylene (HDPE), *Int. J. Mater. Sci. Appl.*, 2013, **2**(3), p 109-114. https://doi.org/10.11648/j.ijmsa.20130203.17
64. E.R. George and J. Reimer, Flamesprayed Thermoplastic Powder Coatings, *Polym. Eng. Sci.*, 1991, **31**(11), p 789-792. https://doi.org/10.1002/pen.760311105
65. J.V. Gulmine, P.R. Janissek, H.M. Heise, and L. Akcelrud, Degradation Profile of Polyethylene after Artificial Accelerated Weathering, *Polym. Degrad. Stab.*, 2003, **79**(3), p 385-397. https://doi.org/10.1016/S0141-3910(02)00338-5
66. P. Guo, M. Wen, L. Wang, and Y. Zheng, Strong Anti-Ice Ability of Nanohairs over Micro-Ratchet Structures, *Nanoscale*, 2014, **6**(8), p 3917-3920. https://doi.org/10.1039/C3NR04061E
67. A.G. Pedroso and D.S. Rosa, Mechanical, Thermal and Morphological Characterization of Recycled LDPE/Corn Starch Blends, *Carbohydr. Polym.*, 2005, **59**(1), p 1-9. https://doi.org/10.1016/j.carbpol.2004.08.018
68. C. Li and S.L. Xiao, Effects on the Properties of Polyethylene Film Aging by Different Methods, *Adv. Mater. Res.*, 2013, **830**, p 49-52. https://doi.org/10.4028/www.scientific.net/AMR.830.49